# Morpho-mineralogical exploration of crop, weed and tree derived biochar

Shaon Kumar Das, Goutam Kumar Ghosh, Ravikant Avasthe, Kanchan Sinha


PII: S0304-3894(20)32360-8

DOI: https://doi.org/10.1016/j.jhazmat.2020.124370

Reference: HAZMAT124370

To appear in: *Journal of Hazardous Materials*

Received date: 2 August 2020
Revised date: 26 September 2020
Accepted date: 21 October 2020

Please cite this article as: Shaon Kumar Das, Goutam Kumar Ghosh, Ravikant Avasthe and Kanchan Sinha, Morpho-mineralogical exploration of crop, weed and tree derived biochar, *Journal of Hazardous Materials,* (2020) doi:https://doi.org/10.1016/j.jhazmat.2020.124370

# Morpho-mineralogical exploration of crop, weed and tree derived biochar

Shaon Kumar Das[a,b*], Goutam Kumar Ghosh[b], Ravikant Avasthe[a] and Kanchan Sinha[c]

[a]*ICAR Research Complex for NEH Region, Sikkim Centre, Gangtok, Sikkim-737102, India*
[b]*Palli Siksha Bhavana, Visva Bharati, Sriniketan, Birbhum, India*
[c]*Indian Agricultural Statistical Research Institute, New Delhi-110012*

*Email for correspondence: shaon.iari@gmail.com (Shaon Kumar Das)
ICAR Research Complex for NEH Region, Sikkim Centre, Gangtok, Sikkim-737102, India
Phone: 03592-231030; Fax: 03592-231238



**ABSTRACT**

It has been quantified the influence of four feedstocks and three pyrolysis temperature on twenty nine morpho-mineralogical characteristics of biochar for their wide range of environmental and soil application. The morpho-mineralogical characteristics were principally manipulated by feedstocks rather than pyrolysis temperature. With increase in pyrolysis temperature the average decrease in biochar mass yield was 20.69%. With increase in pyrolysis temperature the higher heating value of all the four biochar decreased. The X-ray diffraction band patterns of biochar were of an amorphous with crystalline structure and represented significant quartz content. The crystallinity index deceased (average 8.98%) in all biochar with increase in pyrolysis temperature. The presence of crystalline stripes on black dots in transmission electron microscopy proved that the nano-range like sheets was arranged in a tubostratic state. The biochar scanning electron microscopy images showed cross-linked porus structure with layer construction. Low temperature pyrolyzed biochar showed little acid soluble nutrients than high temperature. The existence of more water soluble minerals indicated its potential to act as a source of available plant nutrients. The energy density and energy yield of biochar were linearly and fuel ratio was inversely correlated with pyrolysis temperature.

*Keywords:* Biochar, Energy yield, High heating value, Minerals, Porus structure, Quartz

## 1. Introduction

Biochar is able to sequester carbon along with improved soil health, fertility and plant growth when added in soil and helps to mitigate global climate change (Woolf et al., 2010). The global biomass production from different agricultural sector is about 140 billion tons (Bimbraw et al., 2019). The biomass burning in the fields rises ~70% $CO_2$, 7% CO and 2.1% $NO_2$ and thus biomass burning is considering as a major environmental threat creating health problems and contributing to global warming (NPMCR, 2019). Charring technique also plays a vital role to identify the physico-chemical properties of biochars (Zhao et al., 2018). Zhao et al. (2013) used twelve dried feedstock, heated to 500 $^{o}$C with a heating rate of 18 $^{o}$C $min^{-1}$, hold for 4 h and the biochar recalcitrance was mainly determined by pyrolysis temperature, while the product of recalcitrance and pyrolysis carbon yield depended on feedstocks type. Brewer et al. (2009) found that biochar from hardwood hold more carbon and less ash material than switchgrass and maize stover biochar. Biochar produced from high carbon containing (wood) feedstocks had a lower ash substances and higher C:N ratio than biochar prepared from low carbon biomass like grass, weeds and manure (Mukome et al., 2016).

The physico-chemical characteristics of the source biomass/feedstock and the production unit as well as post-production treatments imposed, show a remarkable responsibility to govern the main functional behaviour of the resultant charcoal, like porosity characteristics, surface charge density, surface area, sorption mechanism, fixed carbon content and mineral nutrient content (Waqas et al., 2018). Tang el al. (2019) produced biochars from vegetable waste, pine cone and their mixture at 200 and 500 °C, and found no heavy metal (HMs) in biochar if HMs is absence in original feedstock and also PAHs were formed during pyrolysis no matter what type of biomass used. Wan et al. (2020) prepared biochars in a tubular furnace, temperature increased till 700 $^{O}$C at a rate of 10 $^{O}$C $min^{-1}$ and maintained for 120 min. The real environmental and soil utility of biochar depends on the characteristics of biochar (Chandra and Bhattacharya, 2019). For application of biochar to be a sustainable endeavor, various regional local biomasses should be converted (Karim et al., 2019). Nevertheless, current investigation on charcoal revealed that its role in the environment and soil is not only concentrated in toxic pollutant removal through adsorption mechanism, but also the dissipation of contaminants by redox reaction by its plentiful

functional groups present on the surface of biochar (Hung et al., 2017). The biochars prepared via facile microwave-assisted carbonization and $CO_2$ activation route can provide a sustainable and high-efficiency carbon electrode (Tang et al. 2020). During the thermochemical conversion of biomass into biochar production, the charring temperature plays a vital function (Kavitha et al., 2018). There is broad variety of pyrolysis technique available such as fast or slow pyrolysis, gasification. It was found that slow pyrolysis process produces more biochar and less bio-oil as compared with fast pyrolysis which produces comparatively less biochar and more bio-oil (Das et al. 2020a).

Compared with low temperature pyrolysis biochar the high temperature product demonstrated less O, H, and contained more aromatic C (Das et al., 2020b). Thus, automatically biochar produced at high temperature pyrolysis process show more resistance and chemical recalcitrance to microbiological and chemical degradation in soil (Al-Wabel wt al., 2017). At present biochar is using in various fields such as climate change mitigation, hazardous waste detoxification, water purification, energy generation and finally field soil fertility amelioration (Cornelissen et al., 2018). Utilizing the low cost biochar as an emerging adsorbent always offers a huge prospective for toxic contaminants removal from polluted water (Tan et al., 2018). Few realistic reasons which can be considered for wide application of biochar for the management of critical environmental problems are (a) very easy to produce from local biomass and low cost (b) can be easily modified to enhancing contaminants removal efficiency and (c) large surface area, total pore volume (Southavong et al., 2018).

There is scarce information available on biochars potentiality produced from indigenous available feedstocks and their description for resourceful exploitation. As a result, experiment was initiated to morpho-mineralogical characterization of weed, tree and crop feedstock derived biochar under three dissimilar pyrolysis temperature (400, 500 and 600 $^{O}$C). Mineralogical composition along with crystallinity index, energy calculation and high heating value (HHV) analysis was conducted to investigate the realistic heterogeneity of biochar to make it ready for soil and environmental application. The XRD, TEM, and SEM analysis were also used to verify the morphological structures like internal fractures, porosity in biochars surface, and mineralogical composition. Such type of data and resources will be of assistance to design engineered biochar for application in soil, environment and industry. The specific objectives

were to explore and judge the morpho-mineralogical composition of biochar that can serve as predictors of their suitability in broader soil and environmental applications.

## 2. Materials and methods

### *2.1 Biomass collection and biochar preparation*

Various types of feedstocks like maize stalk and black gram (crop) was collected from the ICAR-Sikkim Centre Research Farm from previous crop harvesting. The pine needle (tree) and *Lantana camara* (weed) feedstock was collected from the nearby farm area. The research farm was located at 1350 m above the mean sea level (msl) and represents sub-tropical mid hill of Sikkim, India (27˚20'N latitude and 88˚37'E longitude). The Sikkim state of India was declared as first organic state by the Govt of India in 2016. Thus under organic conditions biomass management is a great challenge and conversion them into biochar is a viable option for soil health and environmental application. The feedstock of different sources was shredded to pieces of ≤6 inch and oven dried at 70 $^{o}$C followed by slow pyrolysis into biochar production unit. Charring of all the feedstocks (moisture level ≤5%) was carried out in a portable charring kiln to keep the process quick, low cost and simple. Feedstocks were inserted into the kiln, combusted at 400, 500 and 600$^{o}$C (heating rate 10 $^{o}$C min$^{-1}$ and holding temperature 4 h) and temperature was maintained by electrically operated manual switch. After preparing of biochar they were dried at 100 $^{o}$C (24 h), pulverized to fine powder, sieved through 0.2 mm and used for further characterization.

### *2.2 Biochar mass yield*

The biochar mass yield is simply the ratio of carbonized mass to raw-feedstock mass and thus explains the quantity of the original mass remains in the solid residue of pyrolysis. The percentage of different biochar mass yield (Y) from the method was calculated using the equation (i) as:

$$\text{Yield biochar} = \frac{\text{m biochar}}{\text{m raw}} \times 100\ \% \text{ ---------- (i)}$$

Where Yield biochar = mass yield of biochar, %; m biochar = mass of biochar, kg; m raw = mass of raw biomass, kg.

The produced biochar from different feedstocks denoted by MSB (maize stalk), PNB (pine needles), LCB (*Lantana camara*) and BGB (black gram). The different temperature for each produced biochar denoted by subscript ($B_{400}$, $B_{500}$ and $B_{600}$).

*2.3 Higher heating value (HHV)*

The higher heating value (HHV) is the amount of heat discharged from combusting biomass at an adiabatic oxygen bomb calorimeter in a condensed state, which takes into account the latent heat of vaporization of water in the combustion products. In the absence of bomb calorimeter equipment, estimative via proximate analysis aided with multiple regression formulas is a satisfactory substitute. We have calculated the HHV using the TGA curves and proximate analysis data as per the methods of Parikh et al. (2005). The HVV was calculated as HHV = (0.3536 FC) + (0.1559 VM) - (0.0078 A); where FC is fixed carbon, VM is volatile matter and A is ash content.

*2.4 X-ray diffraction and crystallinity index*

X-ray diffraction (XRD) analysis was used for determination of crystalline constituents of biochar. The XRD plots of the randomly oriented different biochar samples were obtained in a Phillips Xray diffractometer (model PW 1710 diffractometer, PW 1729 X-ray generator) with automated powder diffractometer (APD) software. Analysis was done using Ni-filtered Cu-Kα radiation (λ, 0.154184 nm) operating with voltage 40 kV and current 20 mA at a scanning speed of 1.5°2θ $min^{-1}$. Finally, the crystallinity index of biochar was estimated following the equation of Narzari et al. (2017) as: crystallinity index = $(I_{002} - I_{amp})/I_{002}$; wherein, $I_{002}$ is the highest intensity of $I_{002}$ lattice diffraction and $I_{amp}$ is amorphous peak intensity at $2\theta = 23^{o}$.

*2.5 Transmission electron microscope (TEM) and scanning electron microscope (SEM)*

For analysis by transmission electron microscopy (TEM) 2 mg biochar was mixed with 20 mL of 1-methyl-2-pyrrolidone solvent followed by sonication at 53 kHz (30 min) and then centrifuged at 1000 rpm (1 h). Then the C-film coated Cu-grid was generated in a vacuum evaporator (JEOL.JEE-420). The supernatant was dropped onto the C-film coated grid. TEM was carried out with electron microscope (model no- JEM-1011, JEOL) to record different black dots at 200 kV and the digital images were processed. The textural structure as well as surface morphology

of four dissimilar biochar was differentiated by scanning electron microscopy (SEM) instrument (ZEISS 1550VP field emission SEM) with operating condition at 15.0 kV accelerating potential (P.C. 30 HV).

*2.6 Total, acid soluble and water soluble minerals analysis*

Total mineral nutrient such as total K (TK), Ca (Tca), Mg (TMg), P (TP), Fe (TFe), Mn (TMn), Zn (TZn) and Cu (Tcu) composition was estimated by inductively coupled plasma-mass spectrophotometry (ICP-MS) instrument (model: PerkinElmer Nex ION 300 X). We have used modern micro wave digestion system (Anton par microwave 3000) for the sample digestion. Atfirst 0.5 gm each biochar sample was taken into the digestion tube and 2 mL HCl along with 9 mL 69% nitric acid were added. Then the instrument was run for approximately 40 min and after cooling (when the temperature of biochar was reduced) the digested biochar sample were transferred into a volumetric flask (50 mL). Then distilled water was added to make it upto 50 ml and the liquid sample was transferred into narrow mouth bottle followed by analysis. Selenium (SE), sodium (S) and chromium (CR) was also estimated by ICP-MS. Ammonium-N (NH4) was estimated as per the methodology of Keeney and Nelson (1982) and $NO_3^-$ nitrogen (NO3) was analyzed by Devarda's alloy method. Acid soluble mineral nutrients like Ca (ASCa), Mg (ASMg), K (ASK) and P (ASP) in different biochar samples were estimated in the filtrate collected for determination of calcium carbonate equivalent (CCE) as acid soluble minerals. Similarly, the water soluble mineral nutrients like Ca (WSCa), Mg (WSMg), K (WSK) and P (WSP) in biochar sample were estimated by the modified methodology of Yuan et al. (2011).

*2.7 Calculation of energy value*

To evaluate the pyrolysis method efficiency the fuel ratio, energy density, and energy yield of biochar were calculated. The fuel ratio was determined as FR= fixed carbon (%)/volatile matter (%) (Yadav et al., 2019). The energy density was calculated as ED= $HHV_{biochar}/HHV_{feedstock}$ (Bergman et al., 2005) and finally, energy yield as EY (%) = $Y_{biochar} \times$ ED (Bergman et al., 2005); where HHV is the high heating value (MJ/kg) and Y is yield of biochar.

*2.8 Statistical analysis*

Principal component analysis (PCA) and clustering of variables has been carried out using R programming language (R version 3.6.3). The PCA was employed for factor map & clustering of variables and quality of representation of the variables in a given principal components.

## 3. Result and Discussion

*3.1 Biochar yield*

Biochar pyrolysis temperature was the important factor which influences the actual assessment for its soil and environmental function. In general, feedstock with more lignin show higher biochar mass yield. In our experiment four different biochar yields notably changed with reference to pyrolysis temperature and feedstocks types (Fig. 1a). In a general view the woodier the feedstock there was more yield of biomass. An average of 20.69% decrease in yield was observed with increase in pyrolysis temperature. The maximum yield of all the biochar was at 400 $^{o}$C (32.63%) pyrolysis temperature followed by 500 $^{o}$C (29.20%) and minimum at 600 $^{o}$C (25.88%). The highest biochar yield (%) was recorded by PNB (40.5) followed by LCB (37.5), MSB (29.4) and lowest for BGB (23.1) at 400 $^{o}$C. The more yield of PNB was probably due to macromolecular benzene-propane polymer lignin and utmost thermal firmness of extremely cross-linked. There was a reduction of 20.40, 22.13, 21.62 and 23.80% yield in MSB, LCB, PNB and BGB biochar, respectively at 600 $^{o}$C as compared with the biochar yield at 400 °C. Therefore the maximum yield reduction was in BGB and minimum in MSB. The reduction in yield of BGB and MSB could be due to presence of high amount of xylan and cellulose like polysaccharides which are comparatively rich in $O_2$ molecules and pyrolyzed very easily. The lower yield of biochar at higher charring temperature (600 $^{o}$C) attributed to the emission of more gasses like $CH_4$, CO, $CO_2$ (Amonette and Jospeh, 2009) and accelerated chemical thermolysis as well as organic ingredients volatilization of feedstocks (Yuan et al., 2015). The variability in biochar yield was also due to presence of varied quantity of lignocellulosic substances like lignin, cellulose and hemicelluloses in the feedstocks. The yield decrease in all the four biochar with increase in charring temperature may be correlated with volatile matter loss due to thermally fragmentation of volatiles into low molecular weight organic gasses and liquids by thermal decomposition and dehydration of lignocellulosic components (Chandra and Bhattacharya, 2019).

*3.2 Biochar higher heating value (HHV) estimative*

The effect of pyrolysis temperature and feedstock type on high heating value (HHV) has been presented in Fig. 1(b). The higher heating value (HHV) is the most significant parameter which indicates the energetic potential of different feedstocks from diverse sources. Considering the biochar energy use to replace the coal, the HHV of biochar is the most important fuel property. Results showed that the HHV of fresh feedstocks was more (17.93, 19.75, 20.43 and 16.81 MJ/kg for maize stalk, *Lantana camara*, pine needle and black gram fresh feedstock) than its respective produced biochar at three different pyrolysis temperature. With increase in pyrolysis temperature the HHV of all the four biochar decreased constantly in comparison with fresh feedstock. At 600 $^{O}$C the HHV of MSB, LCB, PNB and BGB was 14.21, 15.35, 15.87 and 13.68 MJ/kg, respectively. It is well known that with increase in pyrolysis temperature the ash content in biochar increase due to discharge of various volatile fractions ($CH_4$), $H_2S$, $CO_2$, $SO_2$, CO, and $H_2$ during pyrolysis process. Thus, hardly mineral elements as well as carbonized charcoal remains in the resulting biochar, suggesting that resulting biochar are identified by lower HHV than its actual feedstock. A lower HHV for carbonized digestate at 500 $^{O}$C was observed by Wisniewski et al. (2015). The high mass yield and HHV of biochar are directly interconnected with the pyrolysis temperature. A biochar with acceptable HHV and high mass yield from raw feedstock can represent a high value-added product from the feedstock (Hung et al., 2017). The findings from our experiment showed a superior yield of biochar as well as HHV can increase the use of maize, lantana, pine and black gram feedstock to create zero waste operation. Thus, in conclusion fixed carbon content and ash played an opposite task in HHV potential pointed out that the biochar energy potential is extremely depends on its carbon to oxidation (after pyrolysis) and mineral concentration.

*3.3 X-ray diffraction analysis*

X-ray diffraction (XRD) pattern of different biochar produced at different pyrolysis temperature has been presented in Fig. 2. In MSB the crystallized quartz (Q) was found by two sharp peak at $2\theta$ = 21.37° and $2\theta$ = 27.16°, dolomite [$CaMg(CO_3)_2$] at $2\theta$ = 29.03°, sylvite (KCl) at $2\theta$ = 42.16°, apatite (phosphate mineral) at $2\theta$ = 45.72° and calcite ($CaCO_3$) at $2\theta$ = 49.37° among all three charring temperatures. In MSB irrespective of temperature the peak location was same.

Here quartz was the dominating mineral. A huge quantity of water soluble-K, acid soluble soluble-K and total-K in the entire four biochar sample can justify the sylvite existence as recognized in the XRD. Charring temperature showed no significant control on position of peak but created it sharper as well as symmetrical. Similarly in LCB the presence of quartz (Q) was confirmed at $2\theta$ = 21.37° and $2\theta$ = 27.16°, dolomite (D) at $2\theta$ = 29.03°, sylvite (S) at $2\theta$ = 42.16°, apatite (A) at $2\theta$ = 47.27° and calcite (C) at $2\theta$ = 49.43° among all three charring temperatures. Here the apatite peak was found in slightly higher band than MSB. The peak intensity of LCB for all the minerals was higher than that observed in MSB. In PNB the crystallized quartz (Q) was found at $2\theta$ = 21.37° and $2\theta$ = 27.16°, dolomite at $2\theta$ = 29.03°, sylvite at $2\theta$ = 40.07° and calcite at $2\theta$ = 49.37° among all three charring temperatures. The sylvite peak was more sharp and intense than other biochars' sylvite peak suggested that sylvite was well crystallized. Here the peak band for sylvite shifted from $2\theta$ = 42.16 to 40.07 which could be due to presence of resin (oleo-resin/turpentine) in pine biochar. Here feedstocks type showed significant influence on sylvite peak position. The apatite peak was absent in PNB. Finally in BGB quartz was found (Q) at $2\theta$ = 21.37° and $2\theta$ = 27.16°, sylvite (S) at $2\theta$ = 42.16° and calcite (C) at $2\theta$ = 49.37° among all three charring temperatures. Interestingly in BGB the apatite was found at $2\theta$ = 8.91° which was not found in MSB, LCB and PNB. The formation of calcite mineral at $2\theta$ = 49.37° in BGB was lower and due to which BGB biochar resulted lower pH and CCE among all the other biochar at all three charring temperatures. The peak for dolomite was absent in BGB which was present in other three biochar. The presence of calcium and magnesium mineral were confirmed with the existence of dolomite and calcite in the entire biochars (Wu et al., 2012). With increase in pyrolysis temperature the intensity of the all the peak slightly increased suggesting that the crystallized minerals contents such as quartz, calcite, sylvite and dolomite increased in all the biochar. Further increasing temperature enhanced in symmetry and band formations. The peak for quartz (Q) was more intense in BGB followed by PNB, LCB and least in MSB which indicated that black gram biomass is high in $SiO_2$ and maize is low in $SiO_2$. Finally, the band patterns of all the four biochars were of an amorphous with crystalline structure. The unordered structure of the amorphous crystalline made it highly stable and is responsible for recalcitrant biochar at low temperature. Hence, high temperature pyrolyzed biochar is slightly better stable than low temperature biochar due to the creation of aromatic C-ring sheet. The XRD study revealed that all the biochar showed huge quartz with different

minerals having amorphous structure; and thus such type of quartz based biochar can be used in biodiesel generation, catalytic industries and deduction of pollutants. Correspondingly biochar with more silica was utilized for biodiesel industries as a catalyst and as an adsorbent for pollutants elimination from liquid oils (Waqas et al., 2018).

*3.4 Crystallinity index of biochar*

The crystallinity index of biochar has a great role on its sorption characteristics, accessibility of microbial population and thus, the crystalline behaviour of biochar is significant. The crystallinity index of four different biochar formed at three pyrolysis temperature has been presented in Fig. 3. The crystallinity index decreased with increase in pyrolysis temperature from the range 400 $^{O}$C to 600 $^{O}$C. At 400 $^{O}$C pyrolysis temperature the crystallinity index was 47.9, 43.2, 41.2 and 38.7% for BGB, PNB, MSB and LCB, respectively. The percentage decrease of crystallinity index at 600 $^{O}$C was 13.78, 8.10, 6.55 and 7.49 % for BGB, PNB, MSB and LCB, respectively with an average decrease 8.98%. Therefore, the biochar generated at higher pyrolysis temperature was slightly more stable due to the formation of aromatic carbon-ring structure and at low pyrolysis temperature was less stable. In our study all the four biochar showed high quartz content and such high quartz based biochar with characters like high mineral content and amorphous structure can be used in catalytic industry, and hazardous poisons elimination via adsorption process. Besides, information on biochar crystallinity index is very useful during its utilization for agricultural applications and bioremediation.

*3.5 Transmission electron microscopy analysis*

Transmission electron microscopy (TEM) analysis of biochar performed for particle size, size distribution and morphology. Transmission Electron Microscopy (TEM) of different biochar produced at different pyrolysis temperature has been presented in Fig. 4. During the magnification process some black dots with nano-range (≤100 nm) particle size of different biochar produced under different temperature on the graphene-like surfaces was seen and these black dots were of crystalline stripes. The presence of crystalline stripes on black dots proved that the nano-range like sheets was haphazardly arranged in a tubostratic state. As carbon is dominant in biochar thus the black dots were resemble to graphene-like structures (Xiao and Chen, 2017). In MSB biochar the particle size was in the range of 6.66-13.32 nm (surface area

12.9-43.9 $m^2$ $g^{-1}$) and it was clearly seen that with increase in charring temperature the particle size was decreased. This can be proved by the fact that at higher charring temperature the BET surface area of biochar also increased. Both surface area and particle size are correlated; and decreased particle size causes increased surface area. The reduced particle size at higher temperature was due to rapid devolatilization which created porous and fragmented chars (Brewer et al., 2009). In LCB biochar the particle size was 8.33-13.46 nm (surface area 12.7-41.4 $m^2$ $g^{-1}$) and here also particle size decreased with increase in charring temperature. Interestingly, here porous region exists and it may be consists of carbon matrix as well as inorganic compounds. In PNB biochar the particle size was 9.40-14.11 nm (surface area 12.5-40.2 $m^2$ $g^{-1}$) and in BGB it was 14.09-35.68 nm (surface area 12.1-38.9 $m^2$ $g^{-1}$) underlying porous carbon matrix. Thus TEM analysis showed that particle size was significantly influenced by feedstock type and charring temperature. The slightly gray fraction of all the four biochar under study was attributed to aromatic clusters having extremely twisted and disordered structures which showed that biochars have disordered stacking.

*3.6 Scanning electron microscopy analysis*

Scanning electron microscope (SEM) of different biochar produced at different pyrolysis temperature has been presented in Fig. 5. Different SEM images discovered that the structure of biochar significantly varied with each other and variation exists in respect to the pyrolysis temperature. The capillary structure of the biochar (produced at 500 and 600 $^oC$) exemplified that the structure was dissimilar than the biochar produced at 400 $^oC$. This result was due to that higher temperature pyrolysis leads to build up the micro pores of biochar at hexagonal planes. This circumstance is associated with the reality wherein the micro pores of biochar brimmed with condensed volatiles tars along with decomposition byproducts, partially arresting the pore space (Bourke et al., 2007). Interestingly, with increase in pyrolysis temperature the pores became prominent and porosity augmented in all the four biochar ensuing better pore properties and it may be due to volatiles escaping during charring process. The MSB showed highest cross-linked pores and feathery-plfate like layer construction on the surface of biochar, mainly the carbonaceous skeleton from the biological capillary structure of the feedstocks, followed by LCB, BGB and PNB. In this experiment the biochar retain few small holes and cracks due to generation of volatile substances during the process of carbonization. The well-established

different pores structure of biochar, with inconsistent surface charge, might promote the methanogenesis procedure at the time of anaerobic digestion along with $CO_2$ discharge and acceleration in $CH_4$ production for upholding the cleaner $CH_4$ production (Waqas et al., 2018). At lower charring temperature (400 $^oC$) the SEM images showed firmly packed and opaque disordered microstructure which was disintegrated at higher charring temperature and thus at higher charring temperature some characteristic pores was monitored. In SEM images at 400 $^oC$ charring temperature some macro and fissures pores was seen in all the feedstocks derived biochar with amorphous structure; with increase in temperature the macro-pores converted into well developed micropores (500 $^oC$) and became enlarged in size with smoother morphology (600 $^oC$) which can serve as a site for microbial habitat and nutrient sorption (Chandra and Bhattacharya, 2019).

*3.7 Mineralogical composition*

Mineral composition analysis of different biochar produced at heterogeneous charring temperature and feedstocks sources have been presented in Table 1. The total potassium, calcium, magnesium, phosphorus, iron, zinc and copper content increased with increase in charring temperature and they were low at 400$^oC$ pyrolysis temperature followed by 500$^oC$ and high at 600$^oC$. All the biochar contained higher Ca and Mg because such nutrients vaporize only at greater than 1000 °C. The richness of different mineral elements like P, Ca, Mg, Fe, Mn, Cu and Zn originated from various feedstocks materials. All the biochar produced by variable pyrolysis temperature contained diverse micronutrients like Fe, Cu, Zn, and Mn whose concentrations are listed in Table 1. Noticeably, all the biochar contained significant amount of P and Ca and such a high concentration of Ca might be due to the bioconversion of organic materials into biogas resulting a predictable liberation of Ca which interacts with $CO_3^-$ or $PO_4^{-3}$ and precipitates (Hung et al., 2017). The $NH_4^+$-N and $NO_3^-$N content in the entire biochar sample reduced with raise in pyrolysis temperature. The decline in the ammonical- and nitrate-nitrogen was due to the elimination of nitrogen by way of volatilization process during the high temperature pyrolysis treatment. Moreover, various nitrogen bearing structures like $–NH_2$, amino-acids and -sugars in biochar were perhaps converted to N-heterocyclic aromatic configuration at higher pyrolytic temperature which reduces the nitrogen content at 600 $^oC$. Accordingly, at higher pyrolysis temperature huge amount of residual nitrogen was possibly

present in biochar as recalcitrant heterocyclic nitrogen and not as easily accessible plant available nitrogen. The highest $NH_4^+$-N content was recorded by BGB (637) followed by MSB (524), LCB (493) and lowest for PNB (436) at 400 $^oC$. Such $NH_4^+$-N content will be equivalent to 1270.81, 1045.38, 983.56 and 869.82 kg/ha, respectively for BGB, MSB, LCB, PNB if we consider field soil. On the other hand, the maximum $NO_3^-$-N was recorded by BGB (1086) followed by MSB (1023), LCB (934) and lowest for PNB (903) at 400 $^oC$. Similarly, such $NO_3^-$ N content will be equivalent to 2166.57, 2040.89, 1863.33, 1801.49 kg/ha, respectively for BGB, MSB, LCB, PNB if we consider field soil. Therefore, due to presence of huge quantity of major available nitrogen mineral for plants the biochar may be regarded as a balanced fertilizer. The $NH_4$-N and $NO_3^-$N are the most important factor for assessing the strength of a biochar for using as emerging soil amendment. Although multiple studies have reported influences of biochar on soil ammonium ($NH_4^+$-N) and nitrate ($NO_3^-$-N), the influences reported are contradictory. For that reason, in order to use the mineral nutrient $NH_4$-N for plant nutrition it is recommended to pyrolyzed the feedstocks at low temperature (400 $^oC$) rather than high temperature (600 $^oC$). The highest total potassium was recorded by MSB (57.1) followed by BGB (53.3), PNB (48.4) and lowest for LCB (45.5) at 600 $^oC$. The total potassium was significantly affected by feedstocks type and pyrolysis temperature and its quantity varied among biochars. The highest total calcium was recorded by MSB (4.74) followed by BGB (4.26), PNB (3.94) and lowest for LCB (3.57). The rising in Ca quantity could be correlated with the high pyrolysis temperature induced volatilization of such minerals**.** The highest total magnesium was recorded by MSB (6.29) followed by BGB (5.73), LCB (4.62) and lowest for PNB (4.17). The highest total phosphorus was recorded by MSB (0.93) followed by LCB (0.81), BGB (0.73) and lowest for PNB (0.53) at 600 $^oC$. Again such rising in Ca could be linked with volatilization of such minerals at higher pyrolysis temperature**.** Such calcium and phosphorus mineral could be present as oxide or calcite forms which can be volatilized or calcined at the high temperature pyrolysis and thus causing compositional and configurationally differences of the produced biochar. The highest iron content was recorded by MSB (7.5) followed by BGB (6.4), LCB (5.1) and lowest for PNB (4.9). The highest total copper was recorded by MSB (6.83) followed by BGB (4.56), PNB (3.96) and lowest for LCB (2.64) at 600 $^oC$. At 600 $^oC$ the highest total zinc was recorded by MSB (9.7) followed by BGB (8.6), PNB (7.8) and lowest for LCB (7.1). Thus, pyrolysis temperature and feedstocks type played a vital responsibility for the differences in micronutrients quantity in the

biochar. The concentration of Cu and Zn were more in all the biochar and thus they can be carefully applied in Cu and Zn deficient agricultural soils. All the biochar also retained significant amount of Fe and this may be due to plants uptake of Fe at the time of its regular growth stage. But with increase in pyrolysis temperature the total manganese content of biochar at first decreased from 400$^{o}$C to 500$^{o}$C and then again increased at 600$^{o}$C significantly. The highest total manganese was recorded by MSB (1.8) followed by BGB (1.6), LCB (1.5) and lowest for PNB (1.4). This reduction in Mn quantity in biochar sample with increase in charring temperature up to 500 $^{o}$C could be linked with biochar pH and CEC.

*3.8 Water and acid soluble mineral nutrients*

Water soluble and acid soluble of different biochar produced at heterogeneous charring temperature and feedstocks sources have been presented in Table 2. The presence of higher amount of water soluble minerals in biochar indicated that the biochar have potential to act as a source of available plant nutrients. All the water soluble minerals such as water soluble potassium, calcium, magnesium and phosphorus increased significantly with increase in pyrolysis temperature. The minerals were low at 400$^{o}$C charring temperature followed by 500$^{o}$C and high at 600$^{o}$C. At 600$^{o}$C the water soluble potassium was more in MSB (34.56) followed by BGB (31.62), LCB (28.58) and lowest in PNB (25.61). The highest water soluble calcium was recorded by MSB (0.76) followed by BGB (0.57), PNB (0.46) and lowest in LCB (0.38) at 600 $^{o}$C. The highest water soluble magnesium was recorded by BGB biochar and lowest for PNB biochar at all pyrolysis temperature. In the water extract the quantity of Mg and Ca were much lower than the concentration of K. The main reason for such high concentration of K was due to the fact that carbonates and oxides of Mg and Ca are very less soluble in water than the carbonates and oxides of K (highly soluble in water). All the biochar showed huge amount of water soluble ions (mainly $K^{+}$) and this verify the higher biochar EC as well as existence of sylvite (KCl). At 600 $^{o}$C the highest water soluble phosphorus was recorded in MSB (2.67) followed by BGB (2.31), PN (1.94) and lowest in LCB (1.82). At 600 $^{o}$C the presence of huge amount of water soluble P indicated that the charcoal can be a promising source for arresting heavy metals due to the fact that P has a tendency to interact with the heavy metals for formation of insoluble P-metal complex [$Pb_5(PO_4)_3Cl$]. The high concentration of water soluble P in biochar would serve as an essential mineral nutrient for plant growth. The reason for higher

amount of water soluble P in biochar was also due to comparatively alkaline pH of all the biochar. Such alkaline biochar pH makes the water soluble P more easily available under alkaline situation where P has a problem to co-precipitated with Mg and Ca. The major enhancement among all the water soluble pool was observed in available K as because biochar contained more total potassium which causes maximum contribution in increasing. The acid soluble mineral such as potassium, magnesium and phosphorus was low at 400 $^{o}$C and increased with increase in charring temperature. The highest acid soluble potassium was recorded by MSB (32.56) followed by BGB (28.62), LCB (24.51) and lowest for PNB (22.56). The highest acid soluble magnesium was recorded by MSB (4.69) followed by BGB (4.17), PNB (3.84) and lowest for LCB (3.78). The highest acid soluble phosphorus was recorded by MSB (3.86) biochar followed by BGB (2.94), PNB (2.37) and lowest for LCB (1.92). But the acid soluble calcium atfirst decrease with increase in charring temperature (500 $^{o}$C) and then again increase at 600$^{o}$C. Thus acid soluble calcium was maximum at 600 $^{o}$C followed by 400 $^{o}$C and minimum at 500 $^{o}$C. The highest acid soluble calcium was recorded by MSB (3.15) biochar followed by BGB (2.73), PNB (2.56) and lowest for LCB (2.37) at 600 $^{o}$C. Low temperature pyrolyzed biochar showed little acid soluble nutrients than high temperature. The acid solubility of all the minerals (K, P, Mg and Ca) modified with pyrolysis temperature. The acid soluble P was more at high temperature pyrolysis and it was due to development of less crystallized phosphorus associated compounds and gain of C. Although Mg showed more acid solubility than P, the former mineral followed a similar trend to P. Therefore, as per the demand, different feedstocks and and pyrolysis temperature can be selected for making the biochar appropriate for exact applications to rectify mineral nutrient deficiency as well as soil quality and productivity (Rehrah et al., 2015).

*3.9 Fuel ratio, energy density and energy yield*

Calculated energy parameters of four different biochar produced at different pyrolysis temperature has been shown in Table 3. With increase in pyrolysis temperature the fuel ratio of all the biochar increased significantly having more fuel ratio in LCB followed by MSB, PNB, and lowest in BGB. The reason was that with increase in pyrolysis temperature the fixed carbon content increased and volatile matter decreased. The energy density and energy yield are linearly correlated. Thus, with increase in pyrolysis temperature the energy density and energy yield (%)

of all the biochar decreased. The reason for decrease in energy density was that with increase in pyrolysis temperature the HHV decreased and thus decrease in energy density. The energy yield was more in PNB followed by LCB, MSB, and lowest in BGB.

*3.10 Principal component analysis*

We have utilized multivariate statistical analysis technique (principal component analysis) to determine the minimum data set (MDS) of most sensitive physical, chemical, ultimate, proximate, carbon, water and acid soluble minerals and mineral composition of different feedstocks derived biochar produced at different pyrolysis temperature. At varying pyrolysis temperature, bivariate Pearson correlation coefficients between the biochar parameters were analysed and based on the correlation co-efficient (r) values their association has been evaluated. In principal component analysis, variables were scaled/standardized in the context of data analysis before PCA and clustering analysis. Only the PCs with eigen values ≥1 were examined. Only the highly weighted variables were retained from each PC for the MDS. Among well correlated variables, the variable with the highest factor loading (absolute value) was chosen for the MDS. Fig. 6 (A-a) represented factor map (component plot) as well as clustering of all the variables which showed the distance between variables and the origin, measures the quality of the variables. Variables which were positively correlated are grouped together whereas negatively correlated variables are positioned on opposite sides of the plot origin. The contributions of variables in accounting for the variability in a given PC can also be assessed from Fig. 6 (B-a). Fig. 6 (A-a) showed that the TMg, TFe, TCa, TCu and TK were highly positively correlated among themselves and thus formed one cluster. The TZn and TMn formed second cluster. The NO3, TP and NH4 formed third cluster based on their similarity. Fig. 6 (B-a) showed that for mineral composition of different biochar the PCA identified two PCs with eigen values > 1.0, altogether accounted for a variation of 75.68% of the total variation present in the original dataset. The PC-1 explained 63.56% variation, having TK, TCa, TFe, TMg and TCu with the highest factor loading as 0.96, 0.95, 0.94, 0.92 and 0.87 respectively. All these variables were highly correlated (r>0.75) and therefore TK was retained and others eliminated from the MDS. The TMn and NO3 were retained from PC-2 (explaining 12.12% variation and low correlation <0.60 with each other) and screened as the most sensitive parameter. Fig. 6 (A-b) showed that the WSMg and WSK were positively correlated with each other and thus formed

one cluster. The WSCa, ASK, ASCa, ASMg and ASP formed one cluster based on their similarity whereas WSP separately formed one cluster. Fig. 6 (B-b) showed that for water & acid soluble minerals in biochar the PCA has identified only one PC with eigen values > 1.0, accounted for a variation of 75.97% of the total variation present in the original dataset. In PC-1 the ASP, ASMg, WSCa, ASK and WSK showed highest factor loading as 0.97, 0.96, 0.94, 0.92 and 0.86, respectively. All these variables were highly correlated (r>0.70) with each other, hence ASP was retained in the MDS as the most sensitive parameter after excluding other parameters.

## 4. Conclusion

The feedstock types and pyrolysis temperature significantly influenced the morpho-mineralogical characteristics of different biomass derived biochar. The biochar mass yield decreased with increase in pyrolysis temperature with highest in PNB followed by LCB, MSB and BGB. The HHV of biochar decreased with increase in pyrolysis temperature due to generation of more ash and volatiles at higher pyrolysis temperature. With increase in pyrolysis temperature the intensity of XRD peak slightly increased suggesting that quartz, calcite, sylvite and dolomite increased in all the biochar with amorphous structure. High quartz based biochar could used in biodiesel generation and catalytic industries. Biochar with satisfactory crystallinity index is useful for agricultural applications, adsorption, and bioremediation. The gray fraction in TEM was due to aromatic clusters having extremely disordered, and particles were in nano range with more surface area. Biochar contained diverse micronutrients (Fe, Cu, Zn, and Mn) and can be used as available plant nutrients in nutrient deficient field soil. Existence of more water- and acid –soluble K, and total-K in biochar can justify the presence of sylvite as recognized in XRD peak. Biochar showed significant amount of P and Ca, and can be used for acid soil reclamation. The well-established pores structure can promote the methanogenesis process. Therefore, during designing a specialized biochar for using in any contexts, pyrolysis temperature and feedstocks are the main factors to be considered that manipulates the real value of biochar for its soil and environmental application.



## Acknowledgements

The first author (Shaon Kumar Das) is thankful to the Director, ICAR Research Complex for NEH Region, Umiam, Meghalaya, India and Department of Soil Science and Agricultural

Chemistry, Palli Siksha Bhavana, Visva Bharati, Shantiniketan, West Bengal, India for providing financial and research work facility during the entire period of study.

**References**

Al-Wabel, M.I., Hussain, Q., Usman, A.R.A., Ahmad, M., Abduljabbar, A., Sallam, A.S., Ok, Y.S., 2017. Impact of biochar properties on soil conditions and agricultural sustainability: A review. Land Degrad. Dev. 29(7), 2124-2161.

Amonette, J.E., Jospeh, S., 2009. Characteristics of biochar: microchemical properties. In: Lehmann J, Joseph S (eds) Biochar for environmental management science and technology. Earthscan. London. 33-43.

Bergman, P., Boersma, A., Kiel, J., Prins, M.J., Ptasinski, K., Janssen, F.J.J.G., 2005. Torrefaction for entrained-flow gasification of biomass. 2nd World. Conf. Technol. Exhib. Biomass. Energy. Ind. Clim. Prot.

Bimbraw, A.S., 2019. Generation and Impact of Crop Residue and its Management. Curr. Agric. Res. J. 7(3), 303-309.

Bourke, J., Manley-Harris, M., Fushimi, C., Dowaki, K., Nunoura, T., Antal, M.J., 2007. Do all carbonized charcoals have the same chemical structure. A model of the chemical structure of carbonized charcoal. Industrial and Engineering. Chemistry Res. 46, 5954-5967.

Brewer, C.E., Schmidt-Rohr, K., Satrio, J.A., Brown, R.C., 2009. Characterization of biochar from fast pyrolysis and gasification systems. Environ. Prog. Sustain. Energy 28(3), 386-396.

Chandra, S., Bhattacharya, J., 2019. Influence of temperature and duration of pyrolysis on the property heterogeneity of rice straw biochar and optimization of pyrolysis conditions for its application in soils. J. Clean. Prod. 215, 1123-1139.

Cornelissen, G., Jubaedah, Nurida, N.L., Hale, S.E., Martinsen, V., Silvani, L., Mulder, J., 2018. Fading positive effect of biochar on crop yield and soil acidity during five growth seasons in an Indonesian Ultisol. Sci. Total. Environ. 634, 561-568.

Das, S.K., Ghosh, G.K., Avasthe, R.K., 2020a. Valorizing biomass to engineered biochar and its impact on soil, plant, water, and microbial dynamics: a review. Biomass Convers. Biorefine. 1-17. https://doi.org/10.1007/s13399-020-00836-5

Das, S.K., Ghosh, G.K., Avasthe, R.K., 2020b. Ecotoxicological responses of weed biochar on seed germination and seedling growth in acidic soil. Environ. Technol. Innov. 101074. https://doi.org/10.1016/j.eti.2020.101074

Hung, C.Y., Tsai, W.T., Chen, J.W., Lin, Y.Q., Chang, Y.M., 2017. Characterization of biochar prepared from biogas digestate. Waste Manage. 66, 53-60.

Karim, A.A., Kumar, M., Mohapatra, S., Singh, S.K., 2019. Nutrient rich biomass and effluent sludge wastes co-utilization for production of biochar fertilizer through different thermal treatments. J. Clean. Prod. 228, 570-579.

Kavitha, B., Reddy, P.V.L., Kim, B., Lee, S.S., Pandey, S.K., Kim, K.H., 2018. Benefits and limitations of biochar amendment in agricultural soils: A review. J. Environ. Manag. 227, 146-154.

Keeney, D. R., Nelson, D. W., 1982. Nitrogen-Inorganic Forms. In A. L. Page (Ed.), Methods of Soil Analysis, Agronomy. Monograph 9. 2, 643-698. Madison, WI: ASA, SSSA.

Mukome, F.N.D., Parikh, S.J., 2016. Chemical, physical, and surface Characterization of biochar. In: Ok, Y.K., Uchimiya, S.M., Chang, S.X., Bolan, N. (Eds.), Biochar: Production, Characterization, and Applications. CRC Press. Boca Raton. FL, USA. 67-96.

Narzari, R., Bordoloi, N., Sarma, B., Gogoi, L., Gogoi, N., Borkotoki, B., Kataki, R., 2017. Fabrication of biochars obtained from valorization of biowaste and evaluation of its physicochemical properties. Bioresour. Technol. 242, 324-328.

NPMCR., 2009. Available online: http://agricoop.nic.in/sites/default/files/NPMCR_1.pdf.

Parikh, J., Channiwala, SA., Ghosal, GK., 2005, A correlation for calculating HHV from proximate analysis of solid fuels. Fuel 84(5), 487-494.

Rehrah, D., Bansode, R.R., Hassan, O., Ahmedna, M., 2015. Physicochemical characterization of biochars from solid municipal waste for use in soil amendment. J. Anal. Appl. Pyrolysis. 118, 42-53.

Southavong, S., Razi, I.M., Preston, T.R., Halimi, M.S., Roslan, I., 2018. Effects of Pyrolysis Temperature and Residence Time on Rice Straw-derived Biochar for Soil Application. Int. J. Plant Soil Sci. 23, 1-11.

Tan, Z., Zou, J., Zhang, L., Huang, Q., 2018. Morphology, pore size distribution, and nutrient characteristics in biochars under different pyrolysis temperatures and atmospheres. J. Mater. Cycles Waste Manag. 20, 1036-1049.

Tang, Yi-Hsin., Liu, Shou-Heng., Tsang, D.C.W., 2020. Microwave-assisted production of $CO_2$-activated biochar from sugarcane bagasse for electrochemical desalination. J. Hazard. Mater. 383, 121192.

Waqas, M., Aburiazaiza, A.S., Miandad, R., Rehan, M., Barakat, M. A., Nizami, A.S., 2018. Development of biochar as fuel and catalyst in energy recovery technologies. J. Clean. Prod. 188, 477-488.

Wisniewski, D., Golaszewski, J., Bialowiec, A., 2015. The pyrolysis and gasification of digestate from agricultural biogas plant. Arch. Environ. Prot. 41, 70-75.

Woolf, D., Amonette, J.E., Street-Perrott, F.A., Lehmann, J., Joseph, S., 2010. Sustainable biochar to mitigate global climate change. Nat. Commun. 1(5), 1-9.

Wu, W., Yang, M., Feng, Q., McGrouther, K., Wang, H., Lu, H., Chen, Y., 2012. Chemical characterization of rice straw-derived biochar for soil amendment. Biomass Bioenerg. 47, 268-276.

Xiao, X., Chen, B., 2017. A Direct Observation of the Fine Aromatic Clusters and Molecular Structures of Biochars. Environ. Sci. Technol. 51(10), 5473–5482.

Yadav, K., Tyagi, M., Kumari, S., Jagadevan, S., 2019 Influence of process parameters on optimization of biochar fuel characteristics derived from rice husk: a promising alternative solid fuel. Bioenergy Res. 12, 1052-1065.

Yang, X., Ng, W., Wong, B.S.E., Baeg, G.H., Wang, Chi-Hwa., Ok, Y.S., 2019. Characterization and ecotoxicological investigation of biochar produced via slow pyrolysis: Effect of feedstock composition and pyrolysis conditions. J. Hazard. Mater. 365, 178-185.

Yuan, H., Lu, T., Huang, H., Zhao, D., Kobayashi, N., Chen, Y., 2015. Influence of pyrolysis temperature on physical and chemical properties of biochar made from sewage sludge. J. Anal. Appl. Pyrolysis 112: 284-289.

Yuan, J.H., Xu, R.K., Zhang, H., 2011. The forms of alkalis in the biochar produced from crop residues at different temperatures. Bioresour. Technol. 102, 3488-3497.

Zhao, L., Cao, X., Masek, O., Zimmerman, A., 2013. Heterogeneity of biochar properties as a function of feedstock sources and production temperatures. J. Hazard. Mater. 256-257, 1–9.

Zhao, N., Lv, Y., Yang, X., Huang, F., Yang, J., 2018. Characterization and 2D structural model of corn straw and poplar leaf biochars. Environ. Sci. Pollut. Res. 25, 25789-25798.

Wana, J., Liu, L., Ayuba, K.S., Zhang, W., Shen, G., Hu, S., Qian, X., 2020. Characterization and adsorption performance of biochars derived from three key biomass constituents. Fuel 269, 117142.

**Figures**

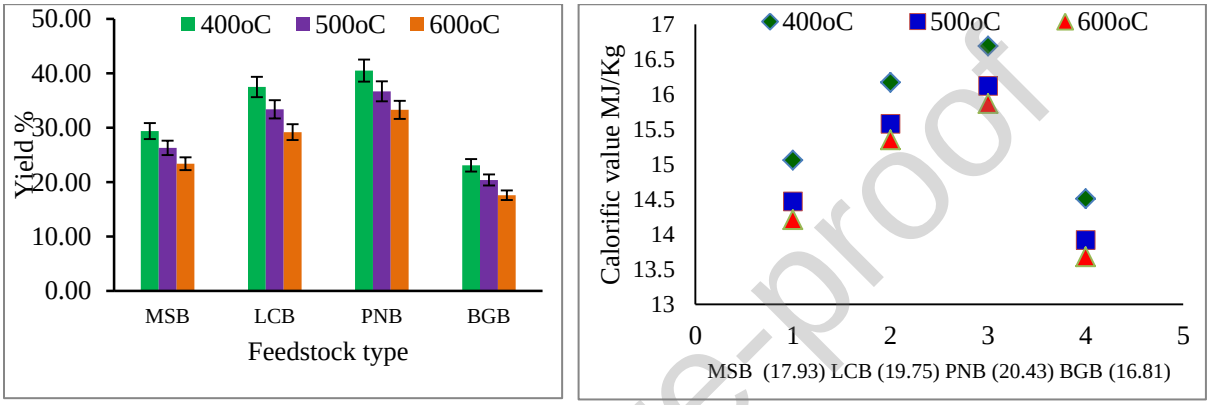


**Fig. 1.** Effect of pyrolysis temperature and feedstock type on a) biochar mass yield and b) calorific value (high heating value) of each biochar (within bracket depicted fresh biomass HHV)

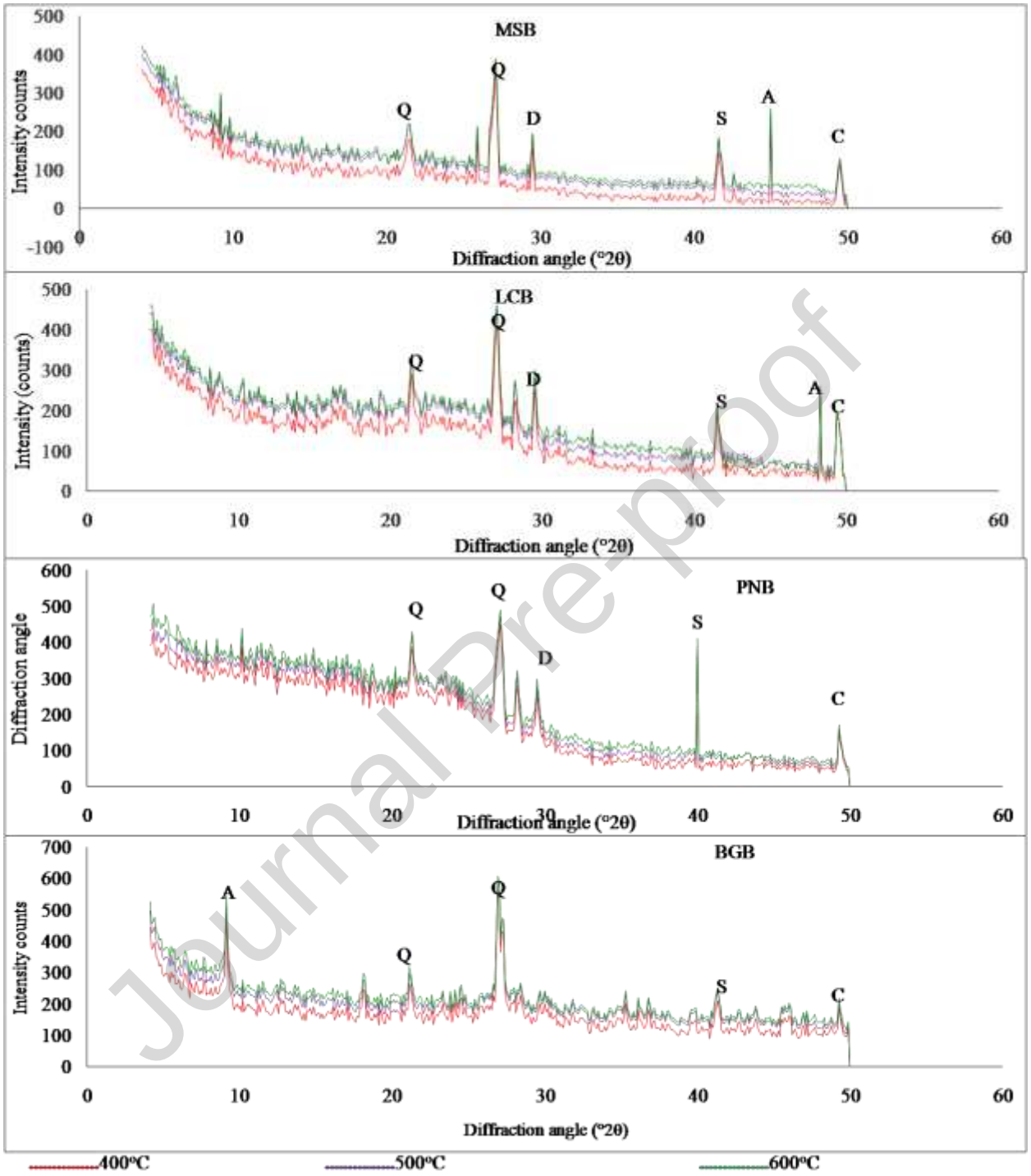




**Fig. 2.** X-ray diffraction (XRD) pattern of different biochar produced at different pyrolysis temperature. *Q* quartz, *C* calcite, *D* dolomite, *S* sylvite, *A* apatite

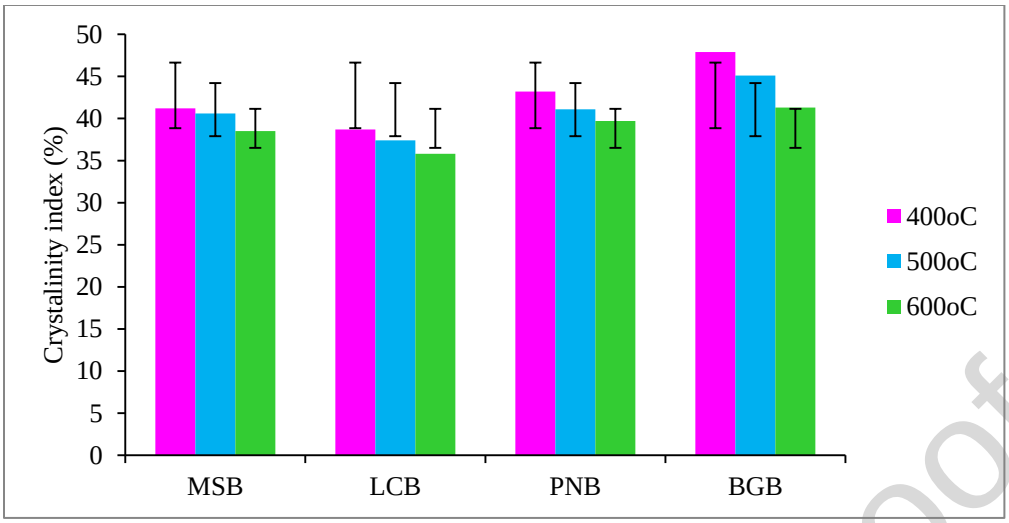


**Fig. 3.** Crystallinity Index of four different biochar formed at three different pyrolysis temperature

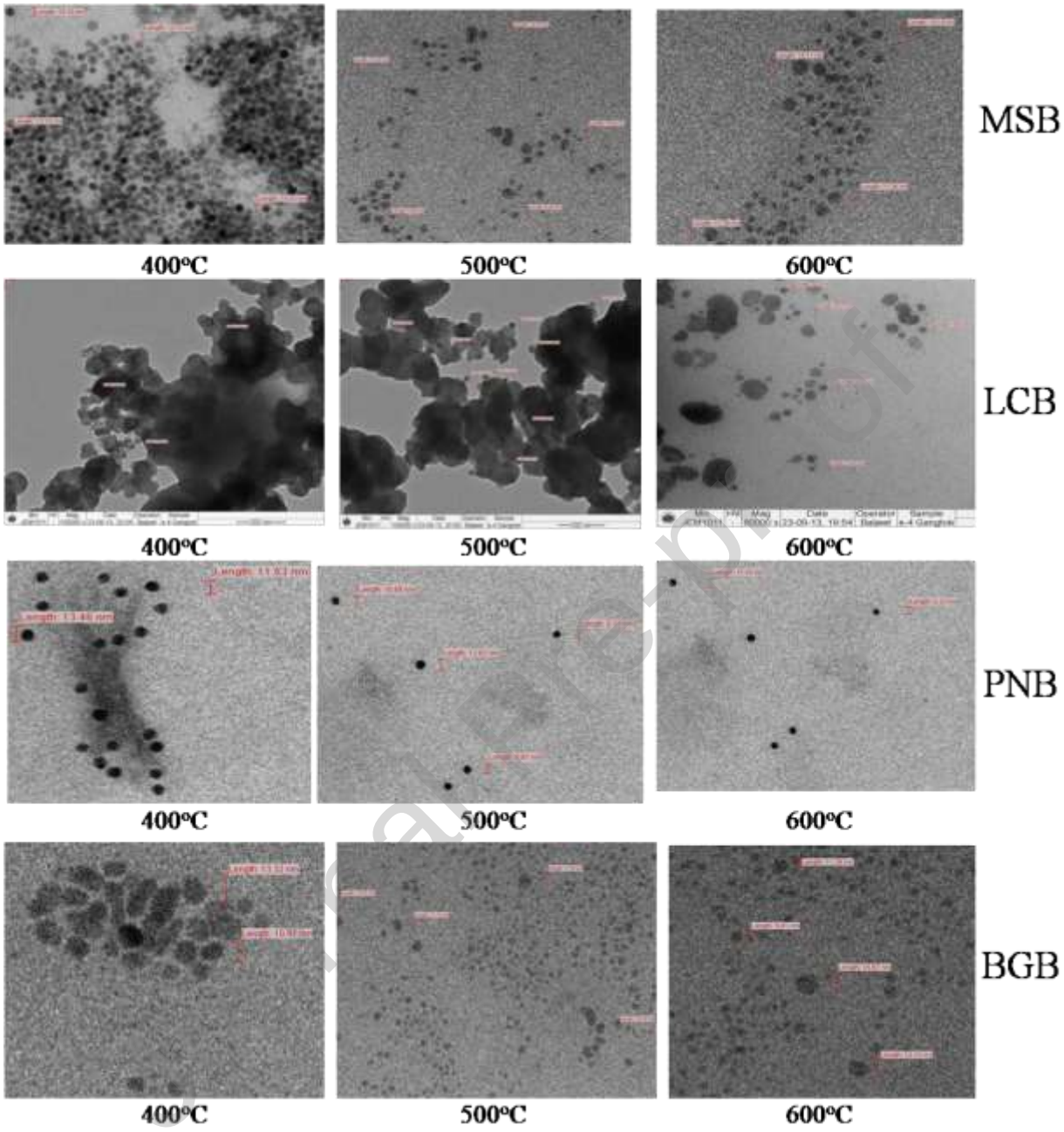


**Fig. 4.** Transmission Electron Microscopy (TEM) of black dots in different biochar produced at different pyrolysis temperature

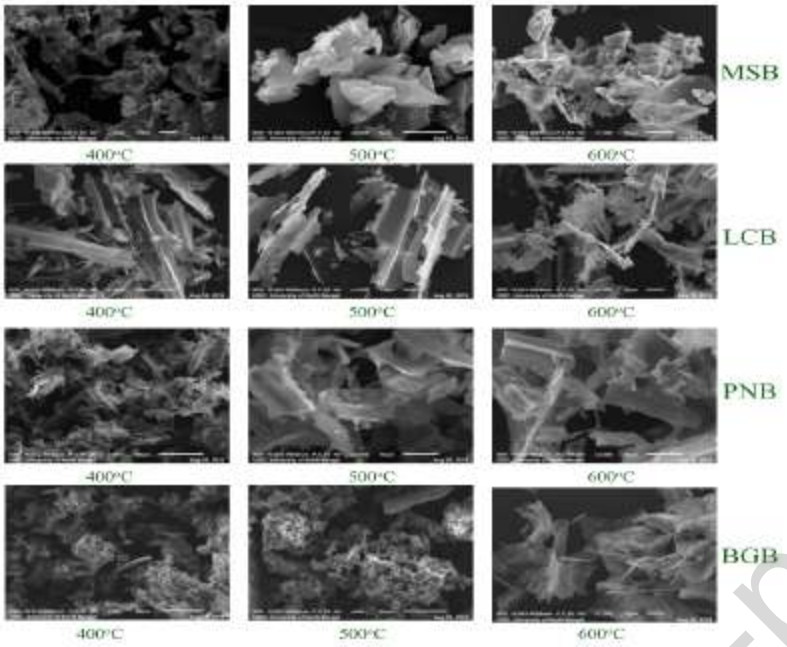


**Fig. 5.** Scanning electron microscope (SEM) of different biochar produced at different pyrolysis temperature

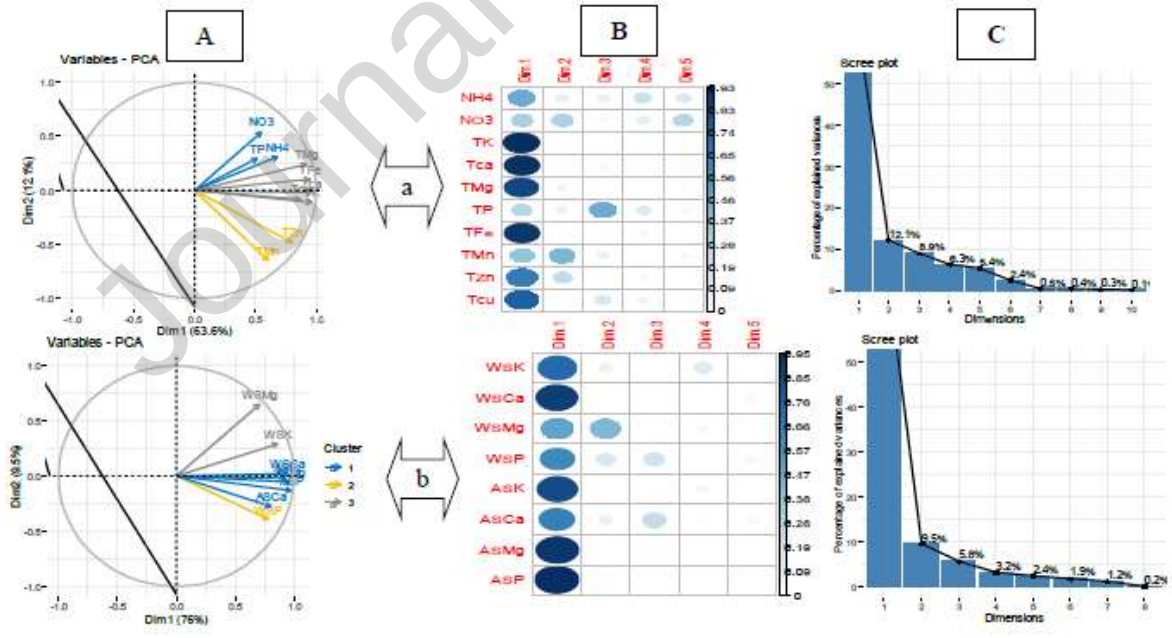


**Fig. 6.** Principal component analysis: (A) factor map & clustering of variables and (B) quality of representation of the variables in a given principal components (C) Scree plot for (a) mineralogical composition (b) water & acid soluble nutrients of different feedstock derived biochar produced at different pyrolysis temperature

**Table 1**.
Mineralogical composition analysis of different biochar produced at heterogeneous charring temperature and feedstocks sources

| Biochar | Temp ($^oC$) | $NH_4^+$-N (mg $kg^{-1}$) | $NO_3^-$-N (mg $kg^{-1}$) | Total potassium TK (g $kg^{-1}$) | Total calcium TCa (g $kg^{-1}$) | Total magnesium TMg (g $kg^{-1}$) | Total phosphorus TP (g $kg^{-1}$) | Total iron TFe (mg $kg^{-1}$) | Total manganese TMn (mg $kg^{-1}$) | Total Zinc TZn (mg $kg^{-1}$) | Total copper TCu (mg $kg^{-1}$) |
|---|---|---|---|---|---|---|---|---|---|---|---|
| MSB | 400 | 524 | 1023 | 48.5 | 4.01 | 5.59 | 0.71 | 6.8 | 1.4 | 5.1 | 4.61 |
| | 500 | 503 | 916 | 52.5 | 4.52 | 6.27 | 0.80 | 7.2 | 1.2 | 6.2 | 6.62 |
| | 600 | 428 | 845 | 57.1 | 4.74 | 6.29 | 0.93 | 7.5 | 1.8 | 9.7 | 6.83 |
| LCB | 400 | 493 | 934 | 36.6 | 3.07 | 4.16 | 0.62 | 4.3 | 1.2 | 3.4 | 1.68 |
| | 500 | 465 | 813 | 41.6 | 3.36 | 4.59 | 0.76 | 4.8 | 1.1 | 3.8 | 2.53 |
| | 600 | 394 | 764 | 45.5 | 3.57 | 4.62 | 0.81 | 5.1 | 1.5 | 7.1 | 2.64 |
| PNB | 400 | 436 | 903 | 41.5 | 2.97 | 3.92 | 0.45 | 4.2 | 1.0 | 4.1 | 2.92 |
| | 500 | 401 | 886 | 43.7 | 3.64 | 4.08 | 0.51 | 4.6 | 0.9 | 4.3 | 3.62 |
| | 600 | 375 | 789 | 48.4 | 3.94 | 4.17 | 0.53 | 4.9 | 1.4 | 7.8 | 3.96 |
| BGB | 400 | 637 | 1086 | 44.6 | 3.61 | 4.98 | 0.53 | 5.6 | 1.2 | 4.3 | 3.39 |
| | 500 | 604 | 983 | 49.3 | 3.89 | 5.67 | 0.68 | 5.9 | 1.0 | 5.1 | 3.46 |
| | 600 | 543 | 892 | 53.3 | 4.26 | 5.73 | 0.73 | 6.4 | 1.6 | 8.6 | 4.56 |

Results of principal components analysis (PCA) of mineral composition of different biochar

| Principal components | PC-1 | PC-2 |
|---|---|---|
| Eigen value[a] variance | 6.35 | 1.21 |
| Per cent cumulative | 63.56 | 12.12 |
| Variance percentage | 63.56 | 75.68 |
| Eigen vectors[b] | | |
| NH4 | .67 | .30 |
| NO3 | .54 | **.53** |
| TK | **.96** | -.10 |
| Tca | **.95** | -.02 |
| TMg | **.91** | .24 |
| TP | .51 | .29 |
| TFe | **.94** | .10 |
| TMn | .60 | **-.65** |
| TZn | .80 | -.47 |
| Tcu | **.86** | -.08 |

* All data were mean of three replicates; ** [a]Eigen values (>1) corresponds to the PCs were considered. [b]Boldface factor loadings were considered highly weighted (>0.40)

**Table 2**.

Water soluble and acid soluble K, Ca, Mg and P of different biochar produced at heterogeneous charring temperature and feedstocks sources

| Biochar | Temp ($^oC$) | Water soluble Potassium WSK ($g\ kg^{-1}$) | Water solubl e calcium WSCa ($g\ kg^{-1}$) | Water soluble magnesium WSMg ($g\ kg^{-1}$) | Water soluble phosphorus WSP ($g\ kg^{-1}$) | Acid soluble potassium ASK ($g\ kg^{-1}$) | Acid solubl e calcium ASCa ($g\ kg^{-1}$) | Acid soluble magnesium ASMg ($g\ kg^{-1}$) | Acid soluble phosphorus ASP ($g\ kg^{-1}$) |
|---|---|---|---|---|---|---|---|---|---|
| MSB | 400 | 23.56 | 0.51 | 1.24 | 2.35 | 30.37 | 2.97 | 4.23 | 3.01 |
| | 500 | 28.25 | 0.59 | 1.37 | 2.45 | 30.89 | 2.57 | 4.57 | 3.52 |
| | 600 | 34.56 | 0.76 | 1.46 | 2.67 | 32.56 | 3.15 | 4.69 | 3.86 |
| LCB | 400 | 20.61 | 0.22 | 1.08 | 1.67 | 22.34 | 2.13 | 3.07 | 1.02 |
| | 500 | 23.67 | 0.27 | 1.25 | 1.73 | 22.97 | 2.07 | 3.63 | 1.38 |
| | 600 | 28.58 | 0.38 | 1.37 | 1.82 | 24.51 | 2.37 | 3.78 | 1.92 |
| PNB | 400 | 16.56 | 0.29 | 1.01 | 1.82 | 20.17 | 2.41 | 3.16 | 1.35 |
| | 500 | 20.67 | 0.36 | 1.12 | 1.91 | 20.93 | 2.17 | 3.72 | 1.89 |
| | 600 | 25.61 | 0.46 | 1.42 | 1.94 | 22.56 | 2.56 | 3.84 | 2.37 |
| BGB | 400 | 21.73 | 0.37 | 1.53 | 2.01 | 26.43 | 2.37 | 3.85 | 2.16 |
| | 500 | 26.56 | 0.48 | 1.65 | 2.12 | 29.96 | 2.26 | 4.06 | 2.67 |
| | 600 | 31.62 | 0.57 | 1.73 | 2.31 | 28.62 | 2.73 | 4.17 | 2.94 |

Results of principal components analysis (PCA) of water soluble and acid soluble K, Ca, Mg and P of different biochar

| Principal components | PC-1 |
|---|---|
| Eigen value[a] variance | 6.07 |
| Per cent cumulative | 75.97 |
| Variance percentage | 75.97 |
| Eigen vectors[b] | |
| WSK | **.85** |
| WSCa | **.94** |
| WSMg | .70 |
| WSP | .77 |
| ASK | **.92** |
| ASCa | .79 |
| ASMg | **.95** |
| ASP | **.97** |

* All data were mean of three replicates; ** [a]Eigen values (>1) corresponds to the PCs were considered. [b]Boldface factor loadings were considered highly weighted (>0.40)

**Table 3**

Energy calculation, BET surface area and average pore diameter of four different biochar produced at different pyrolysis temperature

| Biochar | Temp ($^oC$) | Fuel ratio | Energy density | Energy yield (%) | BET surface area ($m^2\ g^{-1}$) | Average pore diameter (nm) |
|---|---|---|---|---|---|---|

| | | | | | | |
|---|---|---|---|---|---|---|
| MSB | 400 | 1.72 | 0.839 | 24.69 | 12.9 | 2.97 |
| | 500 | 2.33 | 0.807 | 21.22 | 23.2 | 2.71 |
| | 600 | 2.78 | 0.792 | 18.54 | 43.9 | 3.47 |
| LCB | 400 | 1.83 | 0.818 | 30.70 | 12.7 | 2.76 |
| | 500 | 2.46 | 0.788 | 26.35 | 22.1 | 2.45 |
| | 600 | 2.96 | 0.777 | 22.69 | 41.4 | 3.12 |
| PNB | 400 | 1.52 | 0.816 | 33.086 | 12.5 | 2.35 |
| | 500 | 1.84 | 0.789 | 28.96 | 21.8 | 2.01 |
| | 600 | 2.14 | 0.776 | 25.87 | 40.2 | 2.74 |
| BGB | 400 | 1.40 | 0.863 | 19.94 | 12.1 | 3.61 |
| | 500 | 1.73 | 0.828 | 16.89 | 20.4 | 3.04 |
| | 600 | 2.05 | 0.8138 | 14.32 | 38.9 | 3.96 |

Graphical abstract

## CRediT authorship contribution statement

**Shaon Kumar Das:** Complete research work, data interpretation and article writing.

**Goutam Kumar Ghosh:** Research work monitoring, editing manuscript and review.

**R. K. Avasthe:** Research work monitoring, editing manuscript and review.

**Kanchan Sinha:** Statistical analysis (PCA) performed

## Declaration of interests

☐ **The authors declare that they have no known competing financialinterestsor personal relationships that could have appeared to influence the work reported in this paper.**

☐ The authors declare the following financial interests/personal relationships which may be considered as potential competing interests:

**The authors declare that they have no known competing financialinterestsor personal relationships that could have appeared to influence the work reported in this paper.**

**Highlights**

1. Morpho-mineralogical heterogeneity can meet the necessity for application in specific crisis.
2. Higher heating value of biochar decreased constantly with increase in pyrolysis temperature
3. Well-established pores structure of biochar might promote the adsorption process.
4. Crystallized minerals increased with increase in charring temperature
5. Reduced particle size at higher pyrolysis temperature causes increased surface area.